THE JOURNAL OF BIOLOGICAL CHEMISTRY VOL. 286, NO. 34, pp. 30200–30210, August 26, 2011

Activation of the Bumetanide-sensitive Na^+,K^+,$2Cl^-$ Cotransporter (NKCC2) Is Facilitated by Tamm-Horsfall Protein in a Chloride-sensitive Manner*

Received for publication, January 19, 2011, and in revised form, June 7, 2011 Published, JBC Papers in Press, July 7, 2011, DOI 10.1074/jbc.M111.222968

Kerim Mutig[‡1], Thomas Kahl[‡1], Turgay Saritas[‡], Michael Godes[§], Pontus Persson[§], James Bates[¶], Hajamohideen Raffi[¶], Luca Rampoldi[‖], Shinichi Uchida[**], Carsten Hille[‡‡], Carsten Dosche[‡‡], Satish Kumar[¶], Maria Castañeda-Bueno[§§], Gerardo Gamba[§§2], and Sebastian Bachmann[‡3]

*From the Departments [‡]Anatomy and [§]Physiology, Charité-Universitätsmedizin Berlin, 10115 Berlin, Germany, the [¶]University of Oklahoma Health Sciences Center, Oklahoma City, Oklahoma 73104, the [‖]Dulbecco Telethon Institute, Molecular Genetics of Renal Disorders Unit Dibit, San Raffaele Scientific Institute, 20132 Milan, Italy, the **Department of Nephrology, Tokyo Medical and Dental University, Tokyo 113-8519, Japan, the [‡‡]Department of Physical Chemistry, University of Potsdam, 14476 Potsdam, Germany, and the [§§]Instituto de Investigaciones Biomédicas, Universidad Nacional Autónoma de México, Instituto Nacional de Ciencias Médicas y Nutrición Salvador Zubirán, and Instituto Nacional de Cardiología Ignacio Chávez, Mexico City, Distrito Federal 14000, Mexico*

Active transport of NaCl across thick ascending limb (TAL) epithelium is accomplished by Na^+,K^+,$2Cl^-$ cotransporter (NKCC2). The activity of NKCC2 is determined by vasopressin (AVP) or intracellular chloride concentration and includes its amino-terminal phosphorylation. Co-expressed Tamm-Horsfall protein (THP) has been proposed to interact with NKCC2. We hypothesized that THP modulates NKCC2 activity in TAL. THP-deficient mice ($THP^{-/-}$) showed an increased abundance of intracellular NKCC2 located in subapical vesicles (+47% compared with wild type (WT) mice), whereas base-line phosphorylation of NKCC2 was significantly decreased (−49% compared with WT mice), suggesting reduced activity of the transporter in the absence of THP. Cultured TAL cells with low endogenous THP levels and low base-line phosphorylation of NKCC2 displayed sharp increases in NKCC2 phosphorylation (+38%) along with a significant change of intracellular chloride concentration upon transfection with THP. In NKCC2-expressing frog oocytes, co-injection with THP cRNA significantly enhanced the activation of NKCC2 under low chloride hypotonic stress (+112% *versus* +235%). Short term (30 min) stimulation of the vasopressin V2 receptor pathway by V2 receptor agonist (deamino-*cis*-D-Arg vasopressin) resulted in enhanced NKCC2 phosphorylation in WT mice and cultured TAL cells transfected with THP, whereas in the absence of THP, NKCC2 phosphorylation upon deamino-*cis*-D-Arg vasopressin was blunted in both systems. Attenuated effects of furosemide along with functional and structural adaptation of the distal convoluted tubule in $THP^{-/-}$ mice supported the notion that NaCl reabsorption was impaired in TAL lacking THP. In summary, these results are compatible with a permissive role for THP in the modulation of NKCC2-dependent TAL salt reabsorptive function.

The bumetanide-sensitive, apical Na^+,K^+,$2Cl^-$ cotransporter (NKCC2[4] or BSC1; *SLC12A1*) belongs to the family of electroneutral cation-coupled chloride cotransporters and is expressed in the luminal membrane of the thick ascending limb of Henle's loop (TAL; Refs. 1 and 2) where it determines Na^+, K^+, and Cl^- reabsorption (3) and serves to maintain the cortico-medullary osmotic gradient. The fundamental role of NKCC2 in renal salt reabsorption has been firmly established (4–6) and is illustrated by severe salt loss in patients with mutated NKCC (4) as well as by fatal extracellular volume depletion in homozygous NKCC2 knock-out mice (7). Principal mechanisms of NKCC2 activation include modulation of its surface expression (8, 9) as well as phosphorylation of conserved amino-terminal threonines (2, 10) mediated by with no lysine (K) kinases (WNK) and oxidative stress-responsive kinase 1 or STE20/SPS1-related Pro/Ala-rich kinase (5, 11). Vasopressin (AVP) is particularly effective in stimulating NKCC2 via $G\alpha_s$-coupled V2 receptor (V2R; Ref. 10), adenylate cyclase-induced cAMP release, and PKA activation (2, 8, 12, 13). Basal activity of the transporter is dependent on intracellular chloride concentration (14). Mechanisms involved into the intracellular regulation of the transporter are a focus of current research.

NKCC2 is co-localized with Tamm-Horsfall protein (THP, also termed uromodulin), and both are unique products of TAL (15–18). The role of THP has remained obscure for many years, but recent studies have permitted a clearer distinction between

* This work was supported by the Deutsche Forschungsgemeinschaft (FOR 667) and Leducq Foundation and Consejo Nacional de Ciencia y Tecnologia Grant 59992 (to G. G.).

[1] Both authors contributed equally to this paper.

[2] To whom correspondence may be addressed: IIB-INNSZ-INCICH, Vasco de Quiroga 15, Colonia Seccion XVI, Tlalpan, C.P. 14000, Mexico D.F., Mexico. Tel.: 5255-55133868; Fax: 5255-56550382; E-mail: gamba@biomedicas.unam.mx.

[3] To whom correspondence may be addressed: Institut für Vegetative Anatomie, Charité-Universitätsmedizin Berlin, Campus Charité-Mitte, Philippstrasse 12, D-10115 Berlin, Germany. Tel.: 49-30-450-528-001; Fax: 49-30-450-528-922; E-mail: sbachm@charite.de.

[4] The abbreviations used are: NKCC2, Na^+,K^+,$2Cl^-$ cotransporter; V2R, V_2 rho protein receptor; THP, Tamm-Horsfall protein; NCC, NaCl cotransporter; DCT, distal convoluted tubule; dDAVP, deamino-*cis*-D-Arg vasopressin; TAL, thick ascending limb; rbTAL, rabbit TAL cells; HCTZ, hydrochlorothiazide; MQAE, 6-methoxy-quinolyl acetoethyl ester; AVP, vasopressin; WNK, with no lysine (k) kinase; FLIM, fluorescence lifetime imaging microscopy.

its intra- and extracellular functions. The former are related with the urinary concentrating mechanism and potentially interfere with transcellular electrolyte transport (15, 19), whereas the latter have been associated with anti-inflammatory roles of the glycoprotein in the urinary tract and renal interstitium (20–22). Insights into the functional relation between both products have been obtained from gene mutations in humans and from animal models. Mutations of NKCC2 lead to the antenatal variant of Bartter syndrome with severely compromised urinary concentrating ability and reduced expression of THP (4, 23). Mutations of THP are associated with disease (familial juvenile hyperuricemic nephropathy/autosomal dominant medullary cystic kidney disease type 2) characterized by impaired urinary concentration as well (24, 25). In analogy to medullary cystic kidney disease type 2/familial juvenile hyperuricemic nephropathy in humans, chemical induction of a missense mutation in the THP gene produced a mouse line with compromised urinary concentration (26). THP-deficient ($THP^{-/-}$) mice showed moderately impaired urinary concentrating ability; their expression of distal ion transporters and channels including the thiazide-sensitive NaCl cotransporter (NCC) of distal convoluted tubule (DCT) was enhanced, which suggested a compensatory adaptation for putatively insufficient NaCl reabsorption in TAL (15, 27, 28).

We postulate that THP indirectly affects NKCC2-mediated transport function of TAL. This study was designed to evaluate the effects of THP on the mechanisms of NKCC2 activation *in vivo*, in cell culture, and in the *Xenopus* oocyte system and to reveal the putative compensatory adaptation of DCT. Our results suggest a permissive role for THP/uromodulin in TAL reabsorptive function.

EXPERIMENTAL PROCEDURES

Animals, Tissues, Treatments—$THP^{-/-}$ mice and wild-type (WT; $^{+/+}$) controls (15, 20) were bred in the local animal facility and kept on standard diet and tap water. Genotypes of WT and $THP^{-/-}$ mice were confirmed by PCR technique (not shown here; Ref. 15). For morphology studies, adult mice were anesthetized, and the kidneys were perfused retrogradely through the abdominal aorta using 3% paraformaldehyde dissolved in PBS (29), removed, and prepared for cryostat sectioning, standard paraffin sectioning, or ultrastructural resin embedding. For Western blot, mice were killed by an overdose of Nembutal, and the kidneys removed and frozen. Short term vasopressin treatment was administered by intraperitoneal injection of the V2 receptor agonist desmopressin (deamino-*cis*-D-Arg vasopressin (dDAVP); 1 μg/kg of body weight for 30 min; Sigma) or vehicle in adult WT and $THP^{-/-}$ mice.

Cells—Cultured SV40-transformed rabbit TAL cells (rbTAL) obtained from rabbit kidney medulla were cultured as described previously (30). rbTAL cells were transiently transfected with human THP cloned into pcDNA3.1 or GFP-tagged THP (THP-GFP) in pcDNA3.1 vector (31) using FuGENE® HD transfection reagent (Roche Diagnostics) according to the manufacturer's manual. Empty pcDNA3.1 vector or GFP in pcDNA3.1 were applied for control transfections (31). Short term activation (30 min) of the V2R-signaling pathway was performed by combined administration of dDAVP (10^{-7} M) and forskolin (10^{-4} M). For Western blot evaluation cells were harvested, homogenized by sonication, and centrifuged at 1,000 × *g* for 10 min to obtain post-nuclear fractions. For immunohistochemical evaluation cells were fixed in 3% paraformaldehyde/PBS for 20 min.

Intracellular Chloride Recordings—For quantitative intracellular chloride ($[Cl^-]_i$) recordings, two-photon fluorescence lifetime imaging microscopy (FLIM) was performed with the Cl^--sensitive fluorescent dye MQAE (Sigma) as described (32). Briefly, GFP-THP-transfected, GFP-transfected, and non-transfected rbTAL cells were loaded with 10 mM MQAE for 20 min in hypotonic saline. Two-photon fluorescence lifetime imaging microscopy was performed using a MicroTime 200 microscope system (PicoQuant) equipped with a 400–680-nm emission filter and a C-fiber laser (λ_{ex} = 780 nm, 50 MHz, 90-fs pulse width; MenloSystems). Fluorescence was detected by a single-photon avalanche diode. Transfected cells were identified by two-photon-excited GFP fluorescence, and a bandpass filter (450/40 nm) was then added to reject the GFP-signal.

Assessment of the NKCC2 Function—NKCC2 activity was assessed by functional expression in *Xenopus laevis* oocytes as described (5, 14, 33). Oocytes injected with water, NKCC2 cRNA alone (14), THP cRNA alone (31), NKCC2 cRNA + THP cRNA, NKCC2 cRNA + WNK3 cRNA (14), or NKCC2 cRNA + WNK3 cRNA + THP cRNA (each 10 ng/oocyte) were exposed to a low chloride hypotonic stress to promote a decrease in the $[Cl^-]_i$. After injection, oocytes were maintained for 3 days in isotonic ND96 medium (96 mM NaCl, 2 mM KCl, 1.8 mM $CaCl_2$, 1.0 mM $MgCl_2$, and 5 mM HEPES/Tris; 210 mosmol/kg H_2O, pH 7.4). Before the uptake assay, oocytes were incubated overnight either in isotonic or low Cl^- hypotonic stress medium (79 mM sodium isothionate, 2 mM potassium gluconate, 1.8 mM calcium gluconate, 1.0 mM magnesium gluconate, 5 mM HEPES/Tris, 170 mosmol/kg H_2O, pH 7.4). The ensuing $^{86}Rb^+$ uptake experiment included a 30-min preincubation in the control or low Cl^- hypotonic stress medium followed by a 60-min uptake period in a Na^+-, K^+-, and Cl^--containing medium supplemented with 1 mM ouabain in the absence or presence of 0.1 mM bumetanide. At the end of the uptake period, oocytes were washed 5 times in ice-cold uptake solution without isotope, dissolved in 10% sodium dodecyl sulfate, and counted in a β-scintillation counter. Each experiment was performed in duplicate. Because *X. laevis* oocytes express an endogenous Na^+-K^+-$2Cl^-$ cotransporter (5, 8, 14, 33), the mean value observed in oocytes injected with water or THP alone was subtracted to the uptake observed in NKCC2- or NKCC2 + THP-injected oocytes from each experiment.

Furosemide Test—Thirteen- to fourteen-week-old WT and $THP^{-/-}$ mice received a single intraperitoneal injection of vehicle (0.9% saline) or furosemide (40 mg/kg body weight in saline; Sigma). Urine was then collected in metabolic cages for 4 h. Urinary sodium, potassium, chloride, and creatinine concentrations were determined.

Hydrochlorothiazide Test—Thirteen- to fourteen-week-old WT and $THP^{-/-}$ mice were anesthetized with a mixture of ketamine (80 mg/kg body weight) and xylazine (10 mg/kg body weight). After placing the animals on a thermostat table (37 °C), surgical implantation of a tracheal catheter (for sufficient res-

piratory function), an arterial catheter (into the right carotid artery for blood pressure control), and a urinary catheter (into the bladder for urine collection) was performed. To obtain sufficient volumes in the urine fractions, osmotic diuresis was induced by intraarterial infusion of 3.2% mannitol plus 3.2% glucose in water (2 ml/h). Urine fractions were collected every 15 min. After induction of osmotic diuresis, four consecutive urine fractions were collected (fractions 1–4). Vehicle or hydrochlorothiazide (HCTZ; 50 mg/kg body weight; Sigma) were then administered intraperitoneally, and the following six consecutive urine fractions were collected (fractions 5–10). Urinary sodium and potassium concentrations were determined. At the end of the experiments, animals were sacrificed, and plasma samples were obtained to determine electrolytes and osmolality.

Immunohistochemistry—The primary antibodies applied for immunohistochemical labeling of kidney sections and fixed rbTAL-cells were goat anti-THP (ICN Biomedicals), rabbit anti-phospho-NKCC2 (pNKCC2; directed against phosphorylated threonines 95 and 100; Ref. 10), rabbit NCC (provided by D.H. Ellison), and rabbit anti-phospho-NCC (Ser(P)-71-NCC; directed against phosphorylated serine 71; Ref. 34). Signals were generated using immunofluorescence or HRP-based detection as described (10, 29).

Ultrastructural Immunogold Labeling—Mouse kidney tissue was embedded in LR White resin science services, sectioned, and incubated according to established methodology (16) using anti-THP (provided by J. R. Hoyer, Philadelphia, PA), anti-NKCC2 (T4, Developmental Studies Hybridoma Bank; University of Iowa, IA), or anti-phospho-NKCC2 (10) primary antibodies and appropriate secondary antibodies coupled to nanogold particles. Ultrathin sections were viewed with a transmission electron microscope. Quantification of immunogold signal in medullary TAL profiles was performed on micrographs according to an established protocol (35). Gold particles were attributed to the apical cell membrane when located near (within 20 nm of distance) or within the bilayer; particles found below 20 nm of distance to the membrane up to a depth of 2 μm or until the nuclear envelope were assigned to cytoplasmic localization.

Morphometric Procedures—The fractional volume of DCT segments among strains was measured by light microscopy according to previously characterized methods (36, 37). Briefly, 5-μm-thick paraffin sections were stained for NCC whose localization is restricted to the DCT. Cortical areas extending between the renal capsule and the outer medullary boundary were evaluated. Sections were photographed, and a transparent grid with rectangular crossed lines was electronically superimposed on the micrographs; the distances between lines corresponded to 50 μm. The proportion of grid intersections over DCT segments was expressed as the fractional volume of DCT.

Western Blotting—Methods used were as described previously (29, 38). Briefly, kidneys were homogenized in buffer containing 250 mM sucrose, 10 mM triethanolamine, protease inhibitors (Complete; Roche Diagnostics), and phosphatase inhibitors (Phosphatase Inhibitor Mixture 1; Sigma), pH 7.5. The homogenates were subjected to sequential centrifugation steps to obtain post-nuclear fractions (1,000 $\times$ *g*, 15 min), low speed fractions containing large membrane fragments (17,000 $\times$ *g* for 1 h), and high speed fractions enriched in cytoplasmic vesicles (200,000 $\times$ *g* for 1 h). Thirty μg of protein/lane were run on 10% polyacrylamide minigels. After electrophoretic transfer, polyvinylidene fluoride membranes were incubated with specific primary antibodies against NKCC2, pNKCC2, Ser(P)-71-NCC, THP, flotillin-1 (BD Biosciences), or β-actin (Sigma) followed by HRP-conjugated secondary antibodies (Dako Cytomation; 1:3000), induction of chemiluminescence, exposure of x-ray films, and densitometric evaluation.

Statistical Analysis of Data—Experimental data were evaluated by Student's *t* test or the Mann-Whitney U test. $p < 0.05$ was accepted as significant. Values are given as the means $\pm$ S.D. or $\pm$ S.E. where appropriate. Data were analyzed using SPSS for Windows (Version 12.0; SPSS, Chicago, IL).

RESULTS

Steady State Evaluations in TAL and in Frog Oocytes

Cellular Distribution and Phosphorylation of NKCC2—Protein A gold immunocytochemistry was applied to compare the intracellular distribution of NKCC2 in medullary TAL between WT and THP$^{-/-}$ mice. Double-staining with gold particles of different size was performed to analyze topographical relations between NKCC2 and THP. NKCC2 was frequently co-localized with THP in the apical membrane and subapical vesicles at a resolution of less than 10 nm (Fig. 1*a*). Quantification of NKCC2 immunoreactivity in the apical membrane revealed no differences between WT and THP$^{-/-}$ mice, whereas in the subapical vesicle compartment, NKCC2 signal density was significantly higher in THP$^{-/-}$ compared with WT mice (+47%; $p < 0.05$). Accordingly, overall immunogold NKCC2 signal was significantly higher in THP$^{-/-}$ than in WT mice (+27%; $p < 0.05$; Fig. 1, *b–d*). Cellular distribution of NKCC2 was further evaluated by Western blot analysis from cell fractions obtained by either high speed or low speed differential fractionation of kidney homogenates. Densitometric quantification revealed an increase of NKCC2 signal in the vesicle-enriched high speed fractions of THP$^{-/-}$ compared with WT mice (+75%; $p < 0.05$; Fig. 2, *a* and *c*), whereas the low speed fractions were not different. Along with our previous data (15) these results indicate an accumulation of NKCC2 in the subapical vesicular compartment of THP$^{-/-}$ mice.

In contrast to the total NKCC2 levels, phospho-NKCC2 signals were lower in THP$^{-/-}$ compared with WT mice as revealed by Western blot quantification from post-nuclear kidney homogenates (-49%, $p < 0.05$; Fig. 2, *a* and *c*). This was confirmed by immunogold labeling of phospho-NKCC2 showing significantly decreased luminal signal in TAL of THP$^{-/-}$ kidneys (-46%, $p < 0.05$; Fig. 2, *b* and *c*). In cultured rbTAL cells, base-line THP expression was very low to absent. Transient transfection with THP resulted in an ~60% transfection rate (Fig. 3*a*). Phospho-NKCC2 signal in the transfected cells was significantly higher than in controls (+38%; $p < 0.05$; Fig. 3, *b* and *c*). These results suggest that THP facilitates base-line NKCC2 phosphorylation.

Intracellular Chloride Levels—The regulatory influence of intracellular chloride levels ($[Cl^-]_i$) on the phosphorylation and

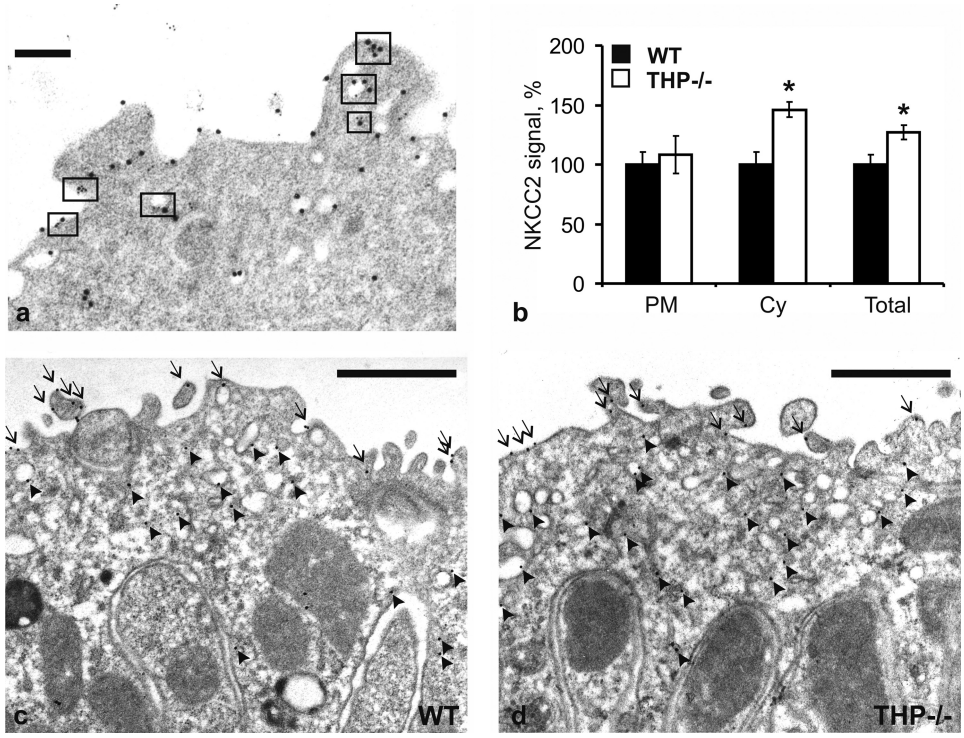

FIGURE 1. **Intracellular distribution of NKCC2 in WT and THP$^{-/-}$ mice (each $n = 3$) as evaluated with protein A-gold immunostaining of medullary thick ascending limbs.** *a*, double immunostaining for THP (5-nm gold particles) and NKCC2 (10-nm gold particles) demonstrates their co-distribution (*rectangular boxes*) within the apical membrane and subapical vesicles (*scale bar* = 0.1 μm). *b–d*, quantification of the NKCC2 signal (*b*) by counting the gold particles on representative micrographs from WT (*c*) and THP$^{-/-}$ mice (*d*) reveals no differences in luminal plasma membrane (*PM*, *arrows*) between strains but significant increases in cytoplasmic vesicles (*Cy*, *arrowheads*) in THP$^{-/-}$ compared with WT mice (*scale bars* = 1 μm). The total NKCC2 signal was accordingly increased in THP$^{-/-}$ mice. At least 10 profiles containing an average of five cells per profile were evaluated per individual. Data are the means ± S.D.; *, $p < 0.05$ for interstrain differences; WT was set at 100%.

activation of NKCC2 has been established (14). To address potential underlying mechanisms of the observed THP-dependent changes in NKCC2 phosphorylation, we evaluated $[Cl^-]_i$ in cultured rbTAL-cells using fluorescence-decay-time-based chloride detection with the Cl^--sensitive dye MQAE. For two-photon FLIM, cells were transfected with GFP-tagged THP and compared with native cells in separate preparations. Transfected cells were identified by two-photon-excited GFP-fluorescence, and a bandpass filter (450/40 nm) was then added to reject the GFP signal. A resting $[Cl^-]_i$ of ~32 mM was observed in the non-transfected cells. $[Cl^-]_i$ was significantly decreased in THP-GFP-transfected cells (−40.4%, $p < 0.01$). Transfection with GFP vector alone did not influence $[Cl^-]_i$ (Fig. 4, *a–d*).

NKCC2 Activation by Low Chloride Hypotonic Stress—Functional consequences of THP transfection upon NKCC2 activity were assessed using the heterologous expression system of *X. laevis* oocytes as this system has been shown to provide a robust and highly reproducible strategy for functional analysis of NKCC2 (3, 5, 8, 14). Oocytes were injected with water, NKCC2 cRNA alone, THP cRNA alone, NKCC2 cRNA + THP cRNA, NKCC2 cRNA + WNK3 cRNA, or NKCC2 cRNA + WNK3 cRNA + THP cRNA. Three days later NKCC2 activity was assessed under basal conditions and after exposing oocytes to a low chloride hypotonic stress, as previously described (14). THP facilitated low chloride hypotonic stress-induced activation of NKCC2 (+112% in the absence of THP *versus* +235% in the presence of THP; $p < 0.01$; Fig. 5*a*). Moreover, THP increased the sensitivity of NKCC2 to intracellular chloride depletion also in the presence of WNK3, a strong activator of NKCC2. In oocytes coinjected with NKCC2 and WNK3, low chloride hypotonic stress induced no further increase of NKCC2 activity, whereas the additional coinjection of THP produced a sharp increase (+286%; $p < 0.01$; Fig. 5*b*).

Effect of Furosemide

To further support our hypothesis of a permissive role of THP for NKCC2-mediated salt reabsorption in TAL, we have studied the effects of furosemide treatment during 4h in WT and THP$^{-/-}$ mice. This resulted in significantly more pronounced increases in sodium excretion in WT compared with THP$^{-/-}$ mice (+462% *versus* +375%; $p < 0.05$), and increases in potassium and chloride excretion were also numerically higher in WT mice. By contrast, the changes in urine flow were similar in both strains (Fig. 6, *a–d*). These results indicate that the effects of furosemide were attenuated in THP$^{-/-}$ mice, which is consistent with a partial decrease of NKCC2 function in the absence of THP.

Vasopressin-induced Effects in TAL

To test the hypothesis that THP facilitates the activation of NKCC2, short term stimulation of the V2R-signaling pathway using the V2R agonist, dDAVP (30 min), or a combination of dDAVP and forskolin (30 min) was performed in mice and in cultured rbTAL cells. In WT mice, dDAVP administration produced significant increases of phospho-NKCC2 in the post-nuclear kidney homogenates (+92%; $p < 0.05$), whereas no changes were found in THP$^{-/-}$ mice (Fig. 7, *a* and *c*). THP-transfected rbTAL-cells responded to dDAVP + forskolin by a significant increase in phospho-NKCC2 signal in post-nuclear

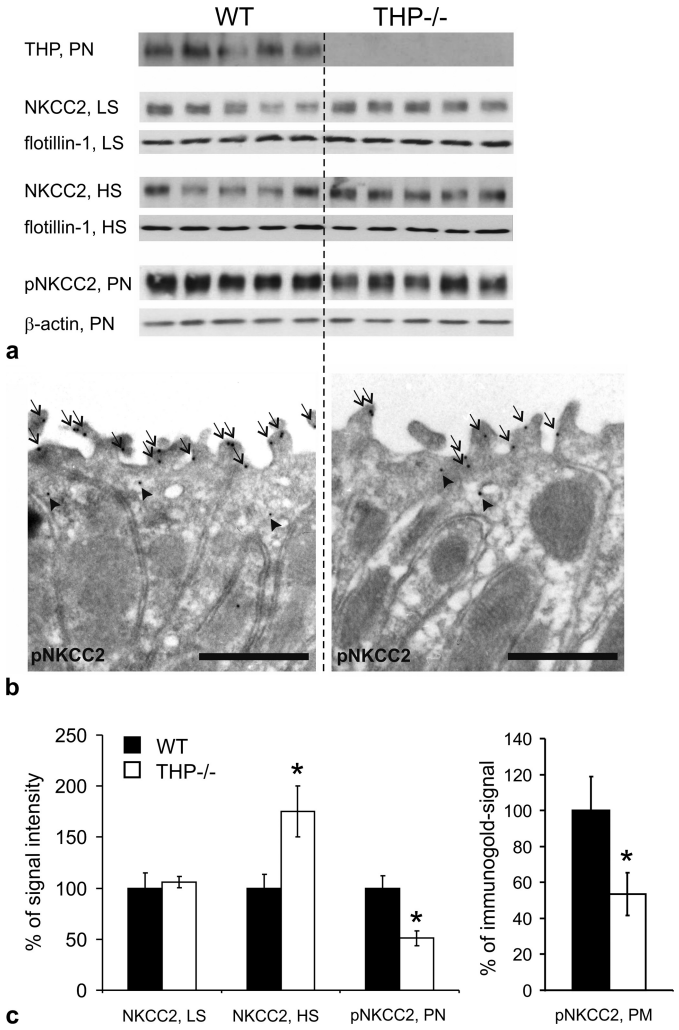

FIGURE 2. **Evaluation of total NKCC2- and phospho (*p*) NKCC2-immunoreactive signals in kidneys of WT and THP$^{-/-}$ mice (each *n* = 5).** *a*, shown are immunoblots of plasma membrane-enriched low speed fractions (*LS*), intracellular vesicle-enriched high speed fractions (*HS*), or post-nuclear fractions (*PN*) from kidneys of WT and THP$^{-/-}$ mice recognized by antibodies directed against THP (~100 kDa), NKCC2 (~160 kDa), and pNKCC2 (~160 kDa) paralleled by appropriate loading controls with antibodies against flotillin-1 (~50 kDa) as a membrane resident protein or β-actin (~40 kDa). *b*, shown is immunogold staining of WT and THP$^{-/-}$ ultrathin kidney sections (medullary thick ascending limbs) for pNKCC2 (6-nm gold particles; signal in luminal plasma membrane, *arrows*; signal in cytoplasmic vesicles, *arrowheads*; *scale bars* = 1 μm). *c*, shown is a densitometric evaluation of immunoreactive signals normalized for the respective loading controls and quantification of pNKCC2 signals in the apical plasma membrane (*PM*) by counting the gold particles on representative micrographs from WT and THP$^{-/-}$ mice (at least 10 profiles containing an average of 5 cells per profile were evaluated per individual). Data are the means ± S.D.; *, $p < 0.05$ for interstrain differences; WT is set at 100%.

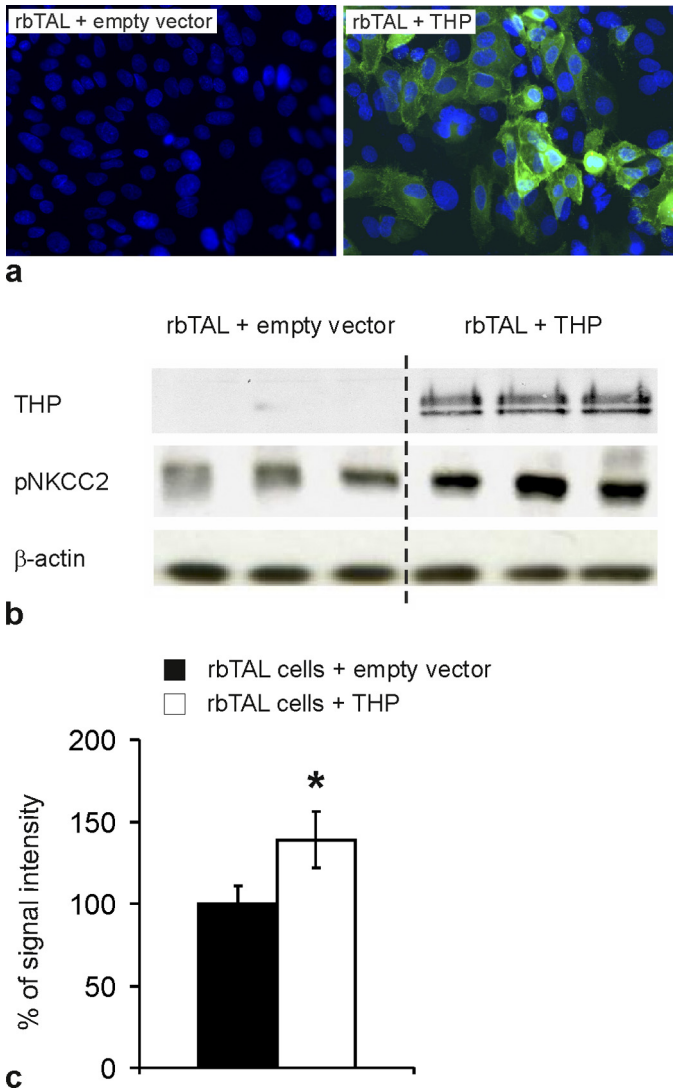

FIGURE 3. **Evaluation of NKCC2 phosphorylation in cultured rbTAL cells transiently transfected with empty vector or THP.** *a*, transfected cells are stained with anti-THP (*green* immunofluorescence), and nuclei are counterstained with DAPI (*blue*); the transient THP-transfection rate was ~60% (original magnification −400). *b*, post-nuclear fractions were detected by anti-THP and anti-pNKCC2 and anti-β-actin as the loading control (representative immunoblots are from three independent experiments). *c*, shown is a densitometric evaluation of pNKCC2 immunoreactive signals normalized for the loading control. Data are the means ± S.D.; *, $p < 0.05$ for differences between THP-transfected and control cells.

homogenates (+67%, $p < 0.05$), whereas cells transfected with control vector showed no change (Fig. 7, *b* and *c*). These data further confirm a role for THP in the activation of NKCC2 by phosphorylation.

Compensatory Changes in DCT

Evaluation of Fractional Volume of DCT and Phosphorylation of NCC—Any chronic deficit in TAL NaCl reabsorption is commonly reflected by compensatory increases of NaCl reabsorption, chiefly in the ensuing DCT segment. The immunoreactive signal intensity for NCC was generally enhanced in DCT of THP$^{-/-}$ compared with WT mice, consistent with previous Western blot data (15). The fractional cortical volume of DCT was compared between strains, revealing a significantly higher proportion of NCC-immunoreactive DCT segments in the cortex of THP$^{-/-}$ compared with WT mice (+40%; $p < 0.05$; Fig. 8, *a*, *b*, and *g*). Apical signal intensity of phospho-NCC was clearly enhanced in THP$^{-/-}$ compared with WT mice (Fig. 8, *c* and *d*). This difference was reflected by a 128% increase in phospho-NCC-signal of the plasma membrane-enriched fractions from THP$^{-/-}$ mice (Fig. 8, *e*, *f*, and *h*). Together, hypertrophy and/or elongation of the DCT along with enhanced phosphorylation of NCC thus corroborate our hypothesis of a compensatory adaptation of DCT in the absence of THP.

Osmotic Diuresis and HCTZ Test—Osmotic diuresis was induced in all mice to obtain sufficiently large urine volumes for

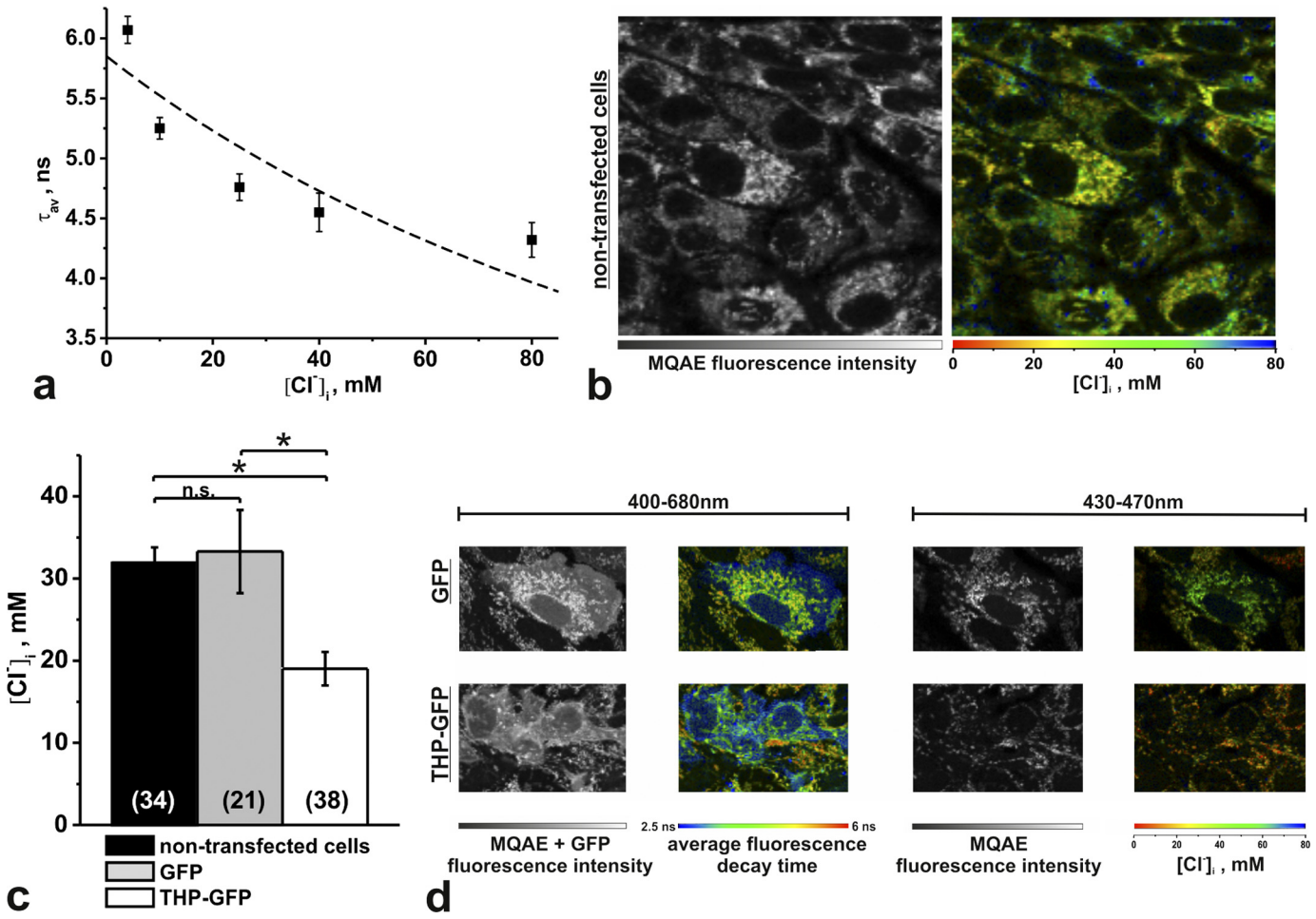

FIGURE 4. **$[Cl^-]_i$ recordings in rbTAL cells using two-photon FLIM and the Cl^--sensitive fluorescent dye MQAE.** *a*, *in situ* calibration using the ionophores tributyltin (40 μM) and nigericin (10 μM) demonstrate the dependence of the MQAE average fluorescence decay time (τ_{av}) on $[Cl^-]_i$. Data were fitted to the Stern-Volmer equation, $\tau_{av} = \tau_{av,0}/(1 + K_{SV}[Cl^-]_i)$, where $\tau_{av,0}$ and τ_{av} are the decay times in the absence and presence of chloride, respectively, and K_{SV} is the Stern-Volmer constant ($n = 4$–9 measurements, each corresponding to one FLIM image covering 10–20 cells). *b*, shown are MQAE fluorescence intensity and a corresponding FLIM image of non-transfected cells (τ_{av} is converted into $[Cl^-]_i$ and shown in false colors; scale 80 × 80 μm). *c*, shown is a statistical comparison (analysis of variance) of resting $[Cl^-]_i$ in non-transfected cells and cells transfected with GFP or THP-GFP (*n.s.*, not significant; *, $p < 0.01$; sample numbers are in *parentheses*). *d*, representative images of GFP- and THP-GFP-transfected cells are shown. Images recorded at 400–680 nm unravel both MQAE and GFP fluorescence and display an additional short fluorescence decay time of GFP (*blue*), which was used to identify and evaluate the transfected cells. Images recorded at 430–470 nm detect only the MQAE fluorescence and allow $[Cl^-]_i$ quantification (*scale*, 25 × 40 μm). Data are the means ± S.E.

urinalysis. Body weight, plasma osmolality, and plasma electrolytes were not different between strains after the administration of vehicle or HCTZ (Table 1). Urine flow was not different between strains during the osmotic diuresis phase as revealed by the four urine fractions that had been collected before treatment and after vehicle application. Administration of HCTZ in $THP^{-/-}$ mice significantly increased the mean urine volume per fraction (+37% in fraction 5 only, $p < 0.05$) without concomitant changes in urine osmolality as compared with the osmotic diuresis phase, whereas no significant changes were seen in WT mice. There were no interstrain differences with respect to mean fractional urine volumes and osmolalities during osmotic diuresis and after the administration of vehicle or HCTZ, respectively. Urinary sodium excretion was not different between strains during the osmotic diuresis phase and after vehicle application except for the last fraction (fraction 10). HCTZ significantly enhanced sodium excretion in both strains compared with vehicle. The initial natriuretic effect (first urine fraction collected after HCTZ injection *versus* the mean value of the 4 fractions from the osmotic diuresis phase) was significantly stronger in $THP^{-/-}$ than in WT mice (+88% in WT *versus* +188% in $THP^{-/-}$ mice, $p < 0.05$). The majority of the remaining fractions after HCTZ also showed higher sodium excretion in $THP^{-/-}$ compared with WT mice (Fig. 9*a*). The cumulative sodium excretion, calculated as the sum of the 6 urine fractions collected after HCTZ, was enhanced in both strains compared with vehicle, and the cumulative natriuretic effect of HCTZ was significantly stronger in $THP^{-/-}$ mice as compared with WT mice (+97%; $p < 0.01$; Fig. 9*b*). Urinary potassium excretion was not different between strains during the osmotic diuresis phase and after vehicle application, whereas the administration of HCTZ, in comparison to vehicle, significantly increased potassium excretion only in $THP^{-/-}$ mice (Fig. 10*a*). Cumulative potassium excretion was enhanced in $THP^{-/-}$ (+38%; $p < 0.05$) but not in WT mice after HCTZ administration, and interstrain differences were absent. To estimate potential compensatory transport adaptations in collecting ducts under HCTZ, the sodium/potassium ratio was

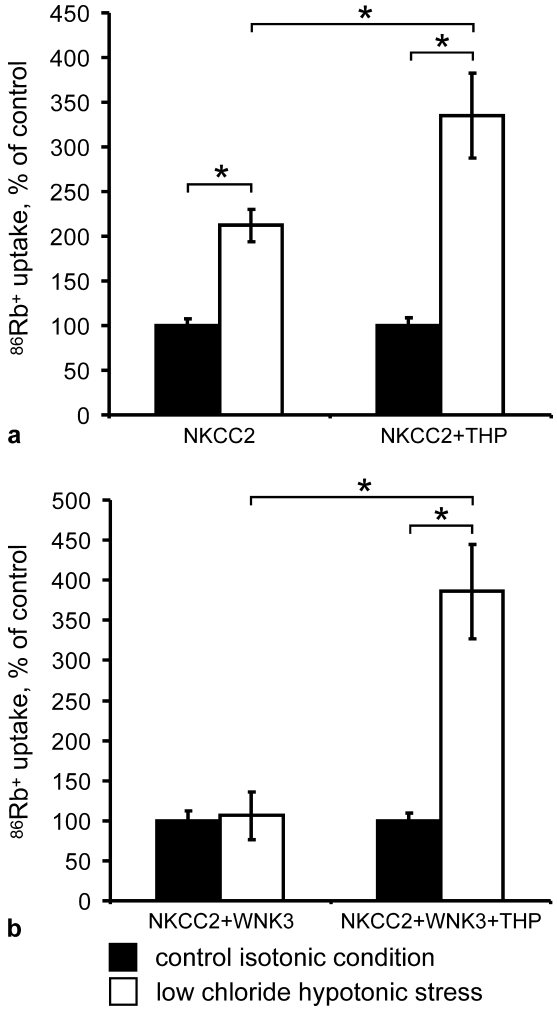

FIGURE 5. **THP facilitates activation of NKCC2 during low chloride hypotonic stress.** *a* and *b*, *Xenopus* oocytes were injected with water or the indicated cRNAs, and the bumetanide-sensitive $^{86}Rb^+$ uptake was measured as described under "Experimental Procedures." The uptake observed in control isotonic conditions (control) was set at 100%, and data recorded under low chloride hypotonic stress were normalized accordingly. Each panel shows the pooled results from two independent experiments with 10 oocytes per group each. Data are the means ± S.E.; *, $p < 0.01$ for differences between the indicated groups.

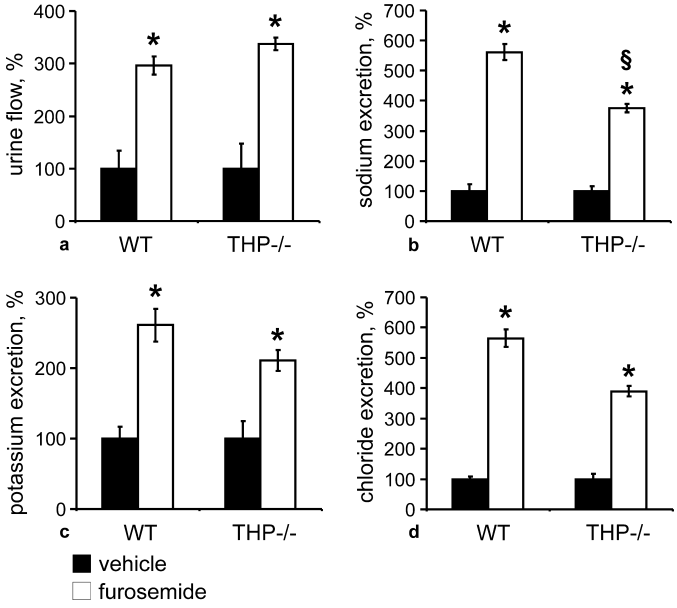

FIGURE 6. **Urinary flow and electrolyte excretion after application of vehicle or furosemide in WT and $THP^{-/-}$ mice (each $n = 10$).** *a–d*, urinary flow (*a*), sodium (*b*), potassium (*c*), and chloride excretion (*d*) obtained from WT and $THP^{-/-}$ mice treated with vehicle or furosemide for 4 h. *, $p < 0.05$ for intrastrain differences between vehicle and furosemide treatments; §, $p < 0.05$ for interstrain differences in the effects of furosemide. Note the significantly attenuated, furosemide-induced natriuresis in $THP^{-/-}$ compared with WT mice (*b*). Data are the means ± S.D. normalized to body weight (*a*) or creatinine excretion (*b–d*). The vehicle group was set at 100%.

calculated. Remarkably, administration of HCTZ induced by far stronger increases in the sodium/potassium ratio in $THP^{-/-}$ compared with WT mice (Fig. 10*b*). This suggests different compensatory capacities of the collecting duct between strains under HCTZ, likely due to persistent activation of the epithelial sodium channel in $THP^{-/-}$ mice (15).

DISCUSSION

Our previous findings on the role of THP had suggested a functionally relevant interaction between THP and transcellular ion transport in TAL (15). $THP^{-/-}$ mice displayed an impaired urinary concentrating ability under water deprivation. The abundances of distal tubular ion transporters or channels such as NCC and epithelial sodium channel were increased at steady state, although blood and urine electrolytes were not altered, suggesting compensatory adjustments by the renal tubule. The present results substantiate the functional relation between NKCC2 and THP; 1) phosphorylation of NKCC2 is modulated by THP likely in a chloride-sensitive manner, 2) activation of NKCC2 via intracellular chloride depletion is increased by cotransfection with THP, 3) effects of furosemide are blunted in $THP^{-/-}$ mice, and 4) DCT displays compensatory adaptation in $THP^{-/-}$ mice, likely reflecting impaired transport within the preceding TAL segment.

Our hypothesis of the role of THP affecting NKCC2-mediated TAL transport function has received substantial support by the present data. Two major criteria suitable to mirror the activity of NKCC2, *i.e.* its abundance at the luminal cell membrane and its phosphorylation state (2, 10), have been applied. While confirming the previously reported increase of total NKCC2 abundance in $THP^{-/-}$ mice (15), the present results have further revealed a disproportionate accumulation of NKCC2 in the subapical vesicle-enriched compartment of the TAL epithelium in $THP^{-/-}$ mice. The luminal abundance of NKCC2 was, however, not different between WT and $THP^{-/-}$ mice so that luminal trafficking of the transporter was probably not impaired. Instead, the subapical accumulation of the transporter in $THP^{-/-}$ mice may reflect an altered turnover, possibly via impaired degradation of NKCC2 in the absence of THP. However, because several other relevant distal transport proteins were enhanced as well (15), an increased intracellular abundance of NKCC2 may also reflect a broader need for compensation of the knock-out. The lack of THP further coincided with decreased steady state levels of phospho-NKCC2 *in vivo* as well as in cell culture, likely reflecting diminished activity of the cotransporter under this condition (2, 5, 11, 14). Along the same line, the present data on a blunted activation of NKCC2 upon stimulation of the V2R-signaling pathway as well as the

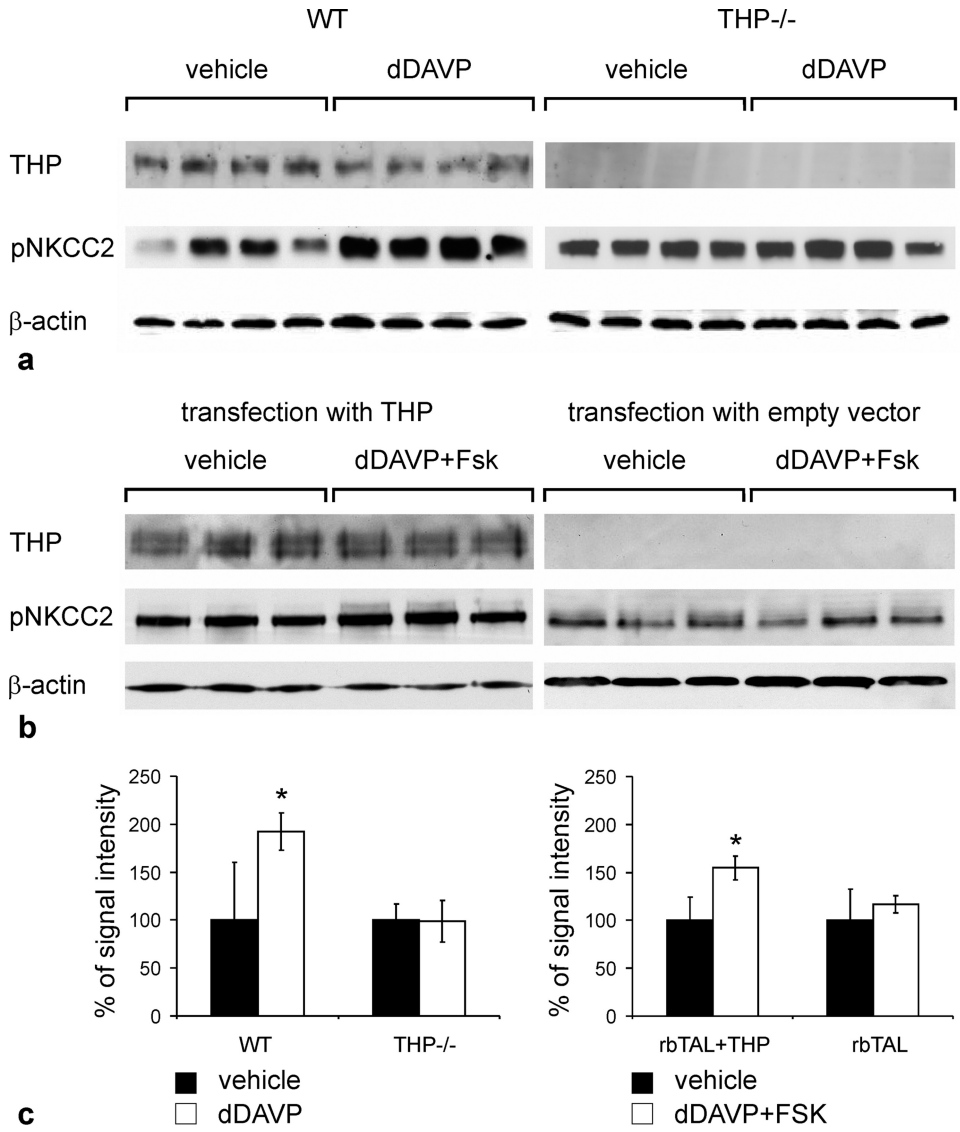

FIGURE 7. **Activation of NKCC2 by short term stimulation of V2 receptor signaling pathway in the presence or absence of THP.** *a* and *b*, immunoblots of post-nuclear fractions from WT and $THP^{-/-}$ mice (each $n = 8$; *a*) or rbTAL-cells transfected with THP or empty vector (*b*) show THP and pNKCC2 and β-actin as the loading control. *c*, shown is a densitometric evaluation of pNKCC2 signals normalized to β-actin. Data are the means ± S.D.; *, $p < 0.05$ for differences between vehicle treatment and stimulation (dDAVP for mice and dDAVP + forskolin (*Fsk*) for rbTAL-cells).

weakened response of $THP^{-/-}$ to furosemide also corroborate an altered NKCC2 function in $THP^{-/-}$ mice.

The mechanism of interaction between THP and NKCC2 is not clear. THP is an abundantly synthesized protein equipped with a glycosylphosphatidylinositol anchor (19). Glycosylphosphatidylinositol-anchored proteins have functions in trafficking of membrane proteins (39) and are ubiquitous components of lipid rafts, in which they may cluster to provide sorting signals for intracellular membrane compartments (30, 39). We have demonstrated close subcellular co-localization of THP and NKCC2, a raft protein itself as well, which suggests that the two proteins may share lipid raft localization (19, 30, 40). Our previous data indicated that activation of NKCC2 is dependent on its presence in lipid rafts (30). Glycosylphosphatidylinositol-anchored THP could, therefore, affect the function of rafts to provide scaffolding platforms that may promote interactions of relevant phosphokinases with NKCC2 (5, 11, 39). These possible interactions may thus serve to explain the failure of NKCC2 to be activated adequately in the absence of THP.

Our results from cultured rbTAL cells have unexpectedly revealed a marked reduction in $[Cl^-]_i$ upon transfection with THP. This may, however, reflect functional activation of NKCC2 nevertheless, since in the setting of an enhanced NaCl transport in medullary TAL induced by cAMP administration, the basolateral membrane conductance, equivalent to the chloride conductance in TAL, was primarily increased in conjunction with decreased transepithelial resistance, which eventually led to reduced $[Cl^-]_i$ levels (41). Along the same line, studies in the *Xenopus* oocyte system have identified the crucial role of a chloride-sensing mechanism in the context of activation of NKCC2 and related NCC by means of phosphorylation. For both transporters, $[Cl^-]_i$ depletion led to an augmented bumetanide/thiazide-sensitive Na^+ uptake; the changes in $[Cl^-]_i$ involved the interaction of distinct WNK isoforms and SPS1-

related Pro/Ala-rich kinase/oxidative stress-responsive kinase 1 kinases to phosphorylate NKCC2 or NCC (14, 33). These observations also imply that in the presence of THP, our finding of low $[Cl^-]_i$ levels at steady state may mirror enhanced transepithelial transport of NaCl triggered by higher NKCC2 phosphorylation as compared with the situation in control rbTAL cells lacking THP. Recently, the apical potassium channel ROMK of TAL was shown to reveal enhanced ROMK current amplitudes measured in *Xenopus* oocytes when co-expressed with THP (42). Therefore, the correction of an insufficient apical K-conductance in THP deficiency by substituting THP may as well help to explain our observations on decreased $[Cl^-]_i$ concentration. In humans, malfunction of this major apical K^+ channel is associated with major reabsorptive defects in TAL causing type II Bartter syndrome (4, 43), which is compatible with reduced basolateral Cl^- conductance.

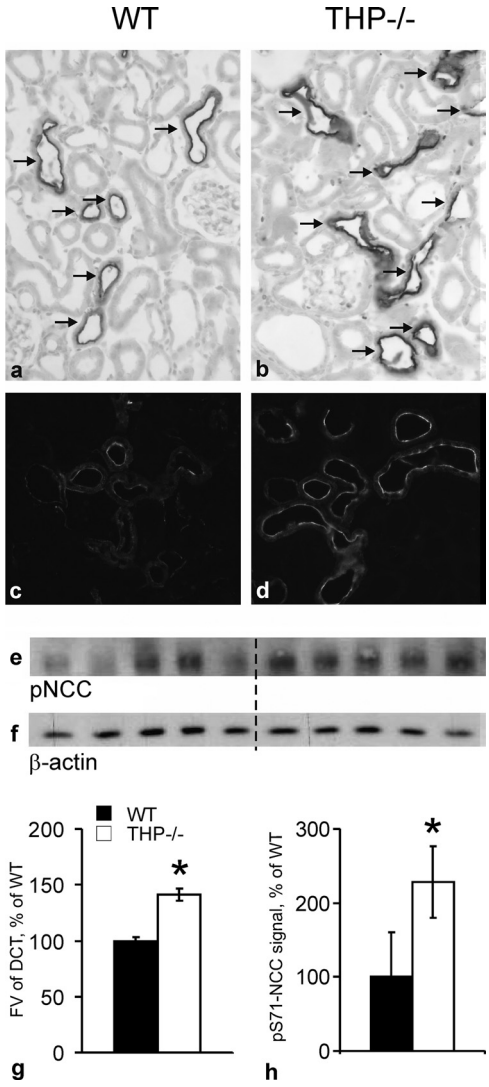

FIGURE 8. **Evaluation of fractional volumes of DCT and phosphorylation of the NCC in kidneys from WT and THP$^{-/-}$ mice (each $n = 4$ and $n = 5$, respectively) at steady state.** *a* and *b*, representative images show a larger proportion of DCT labeled with antibody against NCC in THP$^{-/-}$ than in WT mice (immunoperoxidase staining); *arrows* point to DCT. *c* and *d*, shown is enhanced phosphorylation of NCC in THP$^{-/-}$ mice compared with WT mice by immunostaining against phospho-NCC. *e*, shown are post-nuclear fractions from WT and THP$^{-/-}$ mice detected by Western blot and anti-phospho-NCC antibody (~160 kDa). *f*, shown are loading controls with antibody against β-actin. *g*, shown is morphometric quantification of the fractional volume (*FV*) of DCT. *h*, shown is a densitometric evaluation of phospho-NCC (Ser(P)-71 (*pS71-NCC*)) immunoreactive signals normalized for the loading control. Data are the means ± S.D.; *, $p < 0.05$ for interstrain differences. Original magnification in *a–d*, ×400.

More direct evidence for the facilitating effects of THP on NKCC2-mediated transport is provided by our present *Xenopus* oocyte study. THP enhanced the level of NKCC2 activation by the low chloride hypotonic stress maneuver both in the presence and in the absence of WNK3. Of note, we previously showed that activation of NKCC2 and related NCC by low chloride hypotonic stress is associated with phosphorylation of NKCC2 at the same amino-terminal threonines that become phosphorylated by vasopressin (14, 33).

In aggregate, these considerations point to an insufficient function of NKCC2 and lower sensitivity of the cotransporter to changes in intracellular chloride concentration in the absence of THP. THP appears to facilitate base-line and AVP-induced phosphorylation of NKCC2 by involving a chloride-sensing mechanism. We, therefore, assume that in THP$^{-/-}$ mice, a functional insufficiency of transepithelial NaCl transport occurs along TAL with the exception of the macula densa, which is free of THP by nature (16).

To corroborate our hypothesis we have analyzed the DCT of THP$^{-/-}$ mice for potential compensatory activity, balancing the insufficiency of the preceding TAL. The high effectivity of DCT in this respect has been established and functional as well as structural features of the adaptive response have been demonstrated (27, 28, 36, 37, 44).

At steady state, the measured increases in cortical fractional volume of DCT provides clear evidence for the hypertrophy or elongation of this segment in THP$^{-/-}$ mice. The parallel rise in NCC immunoreactivity in THP$^{-/-}$ agrees with previously reported increases in NCC biosynthesis (15). Because NCC, like NKCC2, is activated by phosphorylation (29, 34, 45), the observed increases in phospho-NCC abundance clearly point to a functional activation of this transporter in THP$^{-/-}$ mice. The present functional data on disproportionally enhanced loss of urinary sodium in THP$^{-/-}$ mice in response to HCTZ further confirms the compensatory role of DCT in THP$^{-/-}$ mice. The significantly higher sodium-to-potassium ratio in THP$^{-/-}$

TABLE 1
Body weight, plasma osmolality, and plasma electrolytes

	Vehicle, WT ($n = 6$)	Vehicle, THP$^{-/-}$ ($n = 9$)	HCTZ, WT ($n = 6$)	HCTZ, THP$^{-/-}$ ($n = 14$)
Body weight, g	29.6 ± 1.2	30.8 ± 3.2	32.5 ± 1.3	32.6 ± 0.7
Plasma osmolality, mosmol/liter	321.0 ± 5.6	317.4 ± 18.5	326.8 ± 7.0	314.1 ± 5.5
Plasma sodium, mmol/liter[a]	118.7 ± 2.5	118.0 ± 12.3	125.0 ± 5.6	121.5 ± 2.7
Plasma potassium, mmol/liter	6.1 ± 0.2	6.38 ± 1.7	4.8 ± 0.4	5.4 ± 0.3

[a] Plasma sodium levels were low probably due to the extensive dilution occurring during prolonged osmotic diuresis. All values are the mean values ± S.E.

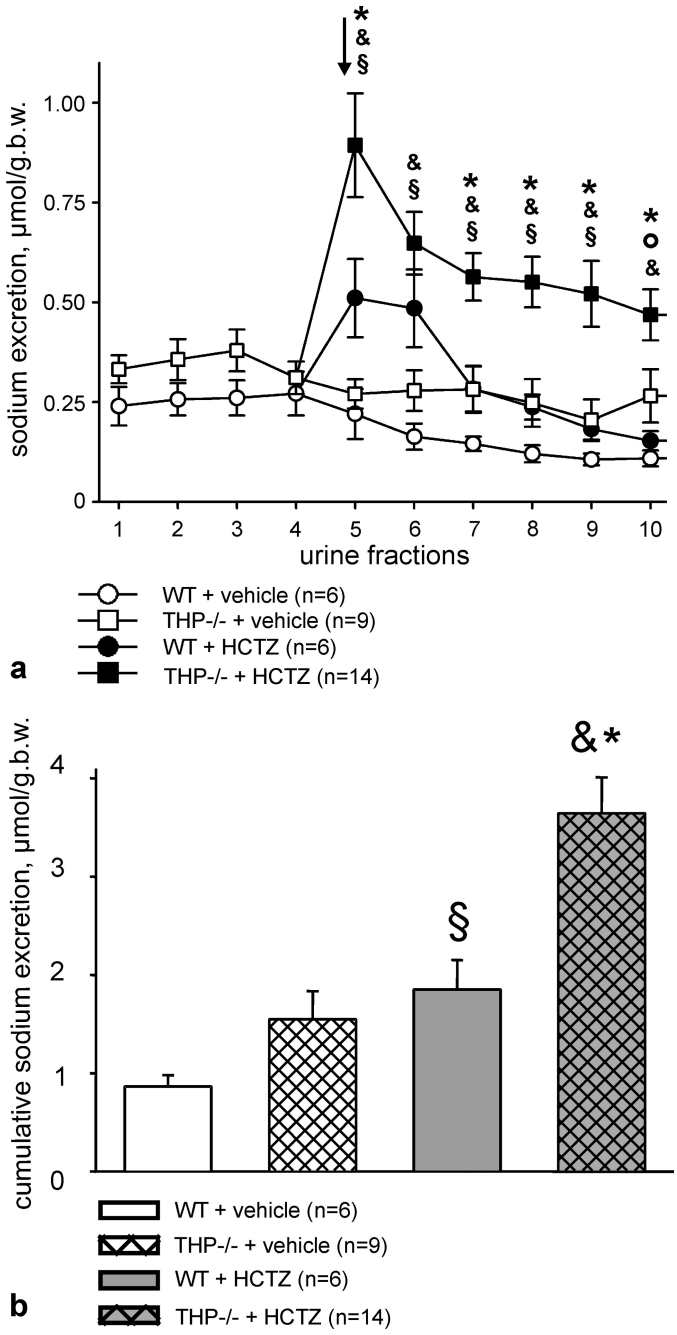

FIGURE 9. **Urinary sodium excretion under osmotic diuresis alone and after additional application of HCTZ or vehicle in WT and THP$^{-/-}$ mice.** *a*, urinary sodium excretion shows the mean values of urine fractions obtained during osmotic diuresis phase (urine fractions *1–4*; WT mice (n = 12), and THP$^{-/-}$ mice (n = 23) and after additional HCTZ or vehicle application (*fractions 5–10* after division of the groups; numbers of individuals are indicated in the diagrams). The *arrow* points to the first urine fraction collected after HCTZ or vehicle treatment. Each fraction was collected within 15 min. *b.w.*, body weight. *b*, shown is cumulative sodium excretion after HCTZ or vehicle application (sum of *fractions 5–10* in *a*). §, $p < 0.05$ for differences between HCTZ- and vehicle-treated WT mice; &, $p < 0.05$ for differences between HCTZ- and vehicle-treated THP$^{-/-}$ mice; °, $p < 0.05$ for differences between vehicle-treated WT and THP$^{-/-}$ mice; *, $p < 0.05$ for differences between HCTZ-treated WT and THP$^{-/-}$ mice. All data are given as the means ± S.E.

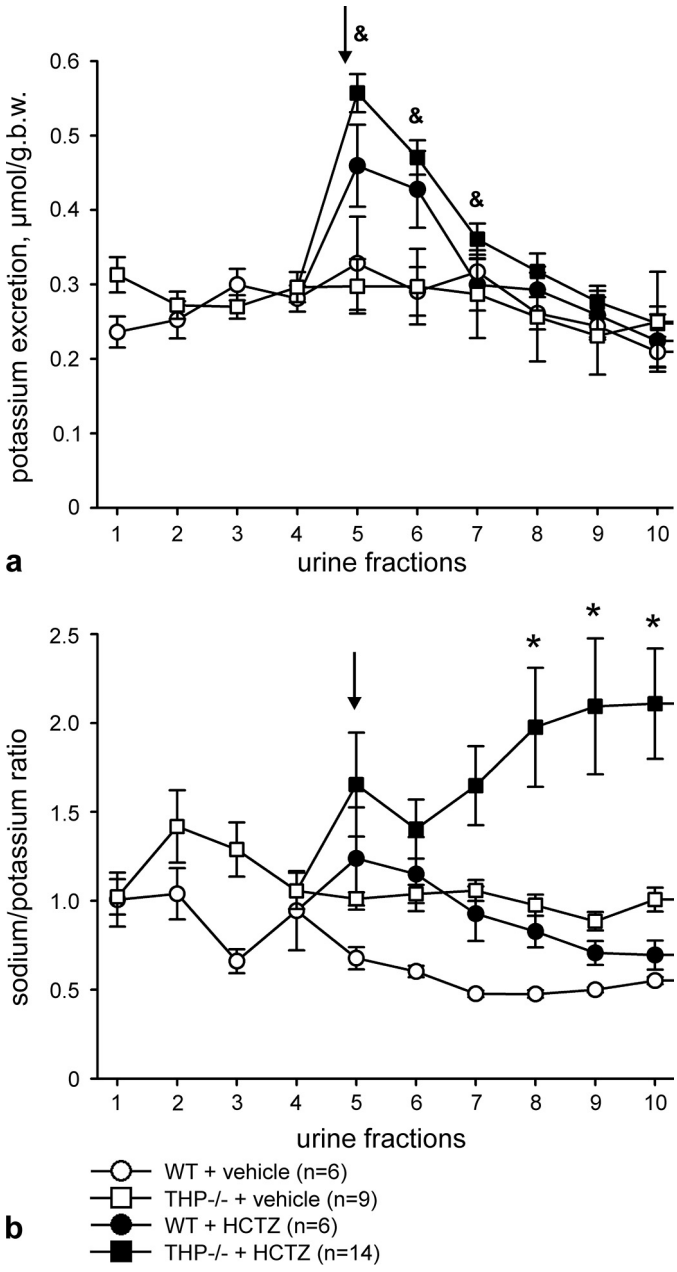

FIGURE 10. **Urinary potassium excretion and sodium/potassium ratio under osmotic diuresis alone and after additional application of HCTZ or vehicle in WT and THP$^{-/-}$ mice.** *a*, urinary potassium excretion shows the mean values of fractions obtained during the osmotic diuresis phase (urine fractions *1–4*; WT mice (n = 12) and THP$^{-/-}$ mice (n = 23)) and after additional HCTZ or vehicle application (*fractions 5–10* after division of the groups; numbers of individuals are indicated in the diagrams). The *arrow* points to the first urine fraction collected after HCTZ or vehicle treatment. Each fraction was collected within 15 min. *b*, in analogy, sodium/potassium ratios are shown as the means of the respective fractions. &, $p < 0.05$ for differences between HCTZ- and vehicle-treated THP$^{-/-}$ mice; *, $p < 0.05$ for differences between HCTZ treated WT and THP$^{-/-}$ mice. For the sodium/potassium ratio, only the differences between HCTZ-treated WT and THP$^{-/-}$ mice are calculated. All data are given as the means ± S.E.

than in WT mice suggests a different compensatory capacity of the collecting duct under HCTZ, likely due to persistent activation of the epithelial sodium channel in THP$^{-/-}$ mice. These results confirm the compensatory role of DCT in THP$^{-/-}$ mice and provide additional evidence for a decreased NaCl transport capacity of their TAL segments. Compared with the drastically impaired renal function in the NKCC2 knock-out mouse (7), however, it may reasonably be assumed that THP-deficient TAL still retains significant residual NKCC2 activity.

Our model presents some major inequities when compared with human defects in THP causing familial juvenile hyperuricemic nephropathy or medullary cystic kidney disease type 2 (24, 25) and a mouse model expressing mutated THP (26). In these studies, markedly compromised urinary concentrating ability associated with THP gene mutations has been proposed to result from the toxic effects of intracellularly accumulated, misfolded protein (24–26, 46). In contrast, $THP^{-/-}$ mice presented normal TAL morphology along with moderately decreased urinary concentrating ability (15).

Collectively, our study suggests that THP is functionally related with NKCC2-mediated NaCl reabsorption in TAL. Two hypotheses were confirmed; 1) activation of NKCC2 is facilitated by THP in a chloride sensitive manner, and 2) in $THP^{-/-}$ mice, structural and functional changes of the DCT indicate compensatory adaption of this segment, presumably in response to an impaired NaCl reabsorption in the preceding, THP-deficient TAL. Our results, therefore, provide convincing support for a role of THP in the functioning of the renal concentrating mechanism. Data may further explain urinary concentration defects in patients with THP/uromodulin mutations.

Acknowledgments—We thank Dr. D. H. Ellison (Portland, Oregon) for providing antibody to NCC, Drs. E. Seeliger and B. Flemming (Berlin) and M. Bleich (Kiel) for discussion of the physiological data, and K. Riskowsky, F. Grams, E. Schindler, M. Gutsmann, C. Riquelme, and N. Vazquez for expert technical assistance.

REFERENCES

1. Obermüller, N., Kunchaparty, S., Ellison, D. H., and Bachmann, S. (1996) *J. Clin. Invest.* **98,** 635–640
2. Giménez, I., and Forbush, B. (2003) *J. Biol. Chem.* **278,** 26946–26951
3. Gamba, G. (2005) *Physiol. Rev.* **85,** 423–493
4. Reinalter, S. C., Jeck, N., Peters, M., and Seyberth, H. W. (2004) *Acta Physiol. Scand.* **181,** 513–521
5. Rinehart, J., Kahle, K. T., de Los Heros, P., Vazquez, N., Meade, P., Wilson, F. H., Hebert, S. C., Gimenez, I., Gamba, G., and Lifton, R. P. (2005) *Proc. Natl. Acad. Sci. U.S.A.* **102,** 16777–16782
6. Schnermann, J. (1998) *Am. J. Physiol.* **274,** R263–R279
7. Takahashi, N., Chernavvsky, D. R., Gomez, R. A., Igarashi, P., Gitelman, H. J., and Smithies, O. (2000) *Proc. Natl. Acad. Sci. U.S.A.* **97,** 5434–5439
8. Meade, P., Hoover, R. S., Plata, C., Vázquez, N., Bobadilla, N. A., Gamba, G., and Hebert, S. C. (2003) *Am. J. Physiol. Renal Physiol.* **284,** F1145–F1154
9. Ortiz, P. A. (2006) *Am. J. Physiol. Renal Physiol.* **290,** F608–F616
10. Mutig, K., Paliege, A., Kahl, T., Jöns, T., Müller-Esterl, W., and Bachmann, S. (2007) *Am. J. Physiol. Renal Physiol.* **293,** F1166–F1177
11. Delpire, E., and Gagnon, K. B. (2008) *Biochem. J.* **409,** 321–331
12. Amlal, H., Legoff, C., Vernimmen, C., Paillard, M., and Bichara, M. (1996) *Am. J. Physiol.* **271,** C455–C463
13. Hebert, S. C., Culpepper, R. M., and Andreoli, T. E. (1981) *Am. J. Physiol.* **241,** F412–F431
14. Ponce-Coria, J., San-Cristobal, P., Kahle, K. T., Vazquez, N., Pacheco-Alvarez, D., de Los Heros, P., Juárez, P., Muñoz, E., Michel, G., Bobadilla, N. A., Gimenez, I., Lifton, R. P., Hebert, S. C., and Gamba, G. (2008) *Proc. Natl. Acad. Sci. U.S.A.* **105,** 8458–8463
15. Bachmann, S., Mutig, K., Bates, J., Welker, P., Geist, B., Gross, V., Luft, F. C., Alenina, N., Bader, M., Thiele, B. J., Prasadan, K., Raffi, H. S., and Kumar, S. (2005) *Am. J. Physiol. Renal Physiol.* **288,** F559–F567
16. Bachmann, S., Koeppen-Hagemann, I., and Kriz, W. (1985) *Histochemistry* **83,** 531–538
17. Bachmann, S., Bostanjoglo, M., Schmitt, R., and Ellison, D. H. (1999) *Anat. Embryol.* **200,** 447–468
18. Nielsen, S., Maunsbach, A. B., Ecelbarger, C. A., and Knepper, M. A. (1998) *Am. J. Physiol.* **275,** F885–F893
19. Malagolini, N., Cavallone, D., and Serafini-Cessi, F. (1997) *Kidney Int.* **52,** 1340–1350
20. Bates, J. M., Raffi, H. M., Prasadan, K., Mascarenhas, R., Laszik, Z., Maeda, N., Hultgren, S. J., and Kumar, S. (2004) *Kidney Int.* **65,** 791–797
21. Mo, L., Zhu, X. H., Huang, H. Y., Shapiro, E., Hasty, D. L., and Wu, X. R. (2004) *Am. J. Physiol. Renal Physiol.* **286,** F795–F802
22. Säemann, M. D., Weichhart, T., Zeyda, M., Staffler, G., Schunn, M., Stuhlmeier, K. M., Sobanov, Y., Stulnig, T. M., Akira, S., von Gabain, A., von Ahsen, U., Hörl, W. H., and Zlabinger, G. J. (2005) *J. Clin. Invest.* **115,** 468–475
23. Schröter, J., Timmermans, G., Seyberth, H. W., Greven, J., and Bachmann, S. (1993) *Kidney Int.* **44,** 401–410
24. Dahan, K., Devuyst, O., Smaers, M., Vertommen, D., Loute, G., Poux, J. M., Viron, B., Jacquot, C., Gagnadoux, M. F., Chauveau, D., Büchler, M., Cochat, P., Cosyns, J. P., Mougenot, B., Rider, M. H., Antignac, C., Verellen-Dumoulin, C., and Pirson, Y. (2003) *J. Am. Soc. Nephrol.* **14,** 2883–2893
25. Hart, T. C., Gorry, M. C., Hart, P. S., Woodard, A. S., Shihabi, Z., Sandhu, J., Shirts, B., Xu, L., Zhu, H., Barmada, M. M., and Bleyer, A. J. (2002) *J. Med. Genet.* **39,** 882–892
26. Kemter, E., Rathkolb, B., Rozman, J., Hans, W., Schrewe, A., Landbrecht, C., Klaften, M., Ivandic, B., Fuchs, H., Gailus-Durner, V., Klingenspor, M., de Angelis, M. H., Wolf, E., Wanke, R., and Aigner, B. (2009) *Am. J. Physiol. Renal Physiol.* **297,** F1391–F1398
27. Abdallah, J. G., Schrier, R. W., Edelstein, C., Jennings, S. D., Wyse, B., and Ellison, D. H. (2001) *J. Am. Soc. Nephrol.* **12,** 1335–1341
28. Wagner, C. A., Loffing-Cueni, D., Yan, Q., Schulz, N., Fakitsas, P., Carrel, M., Wang, T., Verrey, F., Geibel, J. P., Giebisch, G., Hebert, S. C., and Loffing, J. (2008) *Am. J. Physiol. Renal Physiol.* **294,** F1373–F1380
29. Mutig, K., Saritas, T., Uchida, S., Kahl, T., Borowski, T., Paliege, A., Böhlick, A., Bleich, M., Shan, Q., and Bachmann, S. (2010) *Am. J. Physiol. Renal Physiol.* **298,** F502–F509
30. Welker, P., Böhlick, A., Mutig, K., Salanova, M., Kahl, T., Schlüter, H., Blottner, D., Ponce-Coria, J., Gamba, G., and Bachmann, S. (2008) *Am. J. Physiol. Renal Physiol.* **295,** F789–F802
31. Schaeffer, C., Santambrogio, S., Perucca, S., Casari, G., and Rampoldi, L. (2009) *Mol. Biol. Cell* **20,** 589–599
32. Hille, C., Lahn, M., Löhmannsröben, H. G., and Dosche, C. (2009) *Photochem. Photobiol. Sci.* **8,** 319–327
33. Pacheco-Alvarez, D., Cristóbal, P. S., Meade, P., Moreno, E., Vazquez, N., Muñoz, E., Díaz, A., Juárez, M. E., Giménez, I., and Gamba, G. (2006) *J. Biol. Chem.* **281,** 28755–28763
34. Chiga, M., Rai, T., Yang, S. S., Ohta, A., Takizawa, T., Sasaki, S., and Uchida, S. (2008) *Kidney Int.* **74,** 1403–1409
35. Sandberg, M. B., Riquier, A. D., Pihakaski-Maunsbach, K., McDonough, A. A., and Maunsbach, A. B. (2007) *Am. J. Physiol. Renal Physiol.* **293,** F662–F669
36. Ellison, D. H., Velázquez, H., and Wright, F. S. (1989) *J. Clin. Invest.* **83,** 113–126
37. Kaissling, B., Bachmann, S., and Kriz, W. (1985) *Am. J. Physiol.* **248,** F374–F381
38. Sachs, A. N., Pisitkun, T., Hoffert, J. D., Yu, M. J., and Knepper, M. A. (2008) *Am. J. Physiol. Renal Physiol.* **295,** F1799–F1806
39. Paladino, S., Lebreton, S., Tivodar, S., Campana, V., Tempre, R., and Zurzolo, C. (2008) *J. Cell Sci.* **121,** 4001–4007
40. Wilson, B. S., Steinberg, S. L., Liederman, K., Pfeiffer, J. R., Surviladze, Z., Zhang, J., Samelson, L. E., Yang, L. H., Kotula, P. G., and Oliver, J. M. (2004) *Mol. Biol. Cell* **15,** 2580–2592
41. Schlatter, E., and Greger, R. (1985) *Pflügers Arch.* **405,** 367–376
42. Renigunta, A., Renigunta, V., Saritas, T., Decher, N., Mutig, K., and Waldegger, S. (2011) *J. Biol. Chem.* **286,** 2224–2235
43. Welling, P. A., and Ho, K. (2009) *Am. J. Physiol. Renal Physiol.* **297,** F849–F463
44. Na, K. Y., Oh, Y. K., Han, J. S., Joo, K. W., Lee, J. S., Earm, J. H., Knepper, M. A., and Kim, G. H. (2003) *Am. J. Physiol. Renal Physiol.* **284,** F133–F143
45. Richardson, C., Rafiqi, F. H., Karlsson, H. K., Moleleki, N., Vandewalle, A., Campbell, D. G., Morrice, N. A., and Alessi, D. R. (2008) *J. Cell Sci.* **121,** 675–684
46. Choi, S. W., Ryu, O. H., Choi, S. J., Song, I. S., Bleyer, A. J., and Hart, T. C. (2005) *J. Am. Soc. Nephrol.* **16,** 3006–3014